Pseudogaps in Strongly Correlated Metals

M.V.Sadovskii[1], I.A.Nekrasov[1,2], E.Z.Kuchinskii[1], Th.Pruschke[3], V.I.Anisimov[2]

[1]*Institute for Electrophysics, Russian Academy of Sciences, Ekaterinburg, 620016, Russia*

[2]*Institute for Metal Physics, Russian Academy of Sciences, Ekaterinburg, 620219, Russia*

[3]*Institut für Theoretische Physik, Universiät Göttingen, Germany*

Abstract

We generalize the dynamical–mean field (DMFT) approximation by including into the DMFT equations some length scale via a (momentum dependent) "external" self–energy $\Sigma_{\mathbf{k}}$. This external self–energy describes non-local dynamical correlations induced by short-ranged collective SDW–like antiferromagnetic spin (or CDW–like charge) fluctuations. At high enough temperatures these fluctuations can be viewed as a quenched Gaussian random field with finite correlation length. This generalized DMFT+$\Sigma_{\mathbf{k}}$ approach is used for the numerical solution of the weakly doped one–band Hubbard model with repulsive Coulomb interaction on a square lattice with nearest and next nearest neighbour hopping. The effective single impurity problem in this generalized DMFT+$\Sigma_{\mathbf{k}}$ is solved by numerical renormalization group (NRG). Both types of strongly correlated metals, namely (i) doped Mott insulator and (ii) the case of bandwidth $W \lesssim U$ (U — value of local Coulomb interaction) are considered. Densities of states, spectral functions and ARPES spectra calculated within DMFT+$\Sigma_{\mathbf{k}}$ show a pseudogap formation near the Fermi level of the quasiparticle band.

PACS numbers: 71.10.Fd, 71.10.Hf, 71.27+a, 71.30.+h, 74.72.-h

I. INTRODUCTION

Among the numerous anomalies of the normal phase of high–temperature superconductors the observation of a pseudogap in the electronic spectrum of underdoped copper oxides[1,2] is especially interesting. Despite continuing discussions on the nature of the pseudogap, the preferable "scenario" for its formation is most likely based on the model of strong scattering of the charge carriers by short–ranged antiferromagnetic (AFM, SDW) spin fluctuations[2,3]. In momentum representation this scattering transfers momenta of the order of $\mathbf{Q} = (\frac{\pi}{a}, \frac{\pi}{a})$ (a — lattice constant of two dimensional lattice). This leads to the formation of structures in the one-particle spectrum, which are precursors of the changes in the spectra due to long–range AFM order (period doubling). As a result we obtain non–Fermi liquid like behavior (dielectrization) of the spectral density in the vicinity of the so called "hot spots" on the Fermi surface, appearing at intersections of the Fermi surface with antiferromagnetic Brillouin zone boundary[2].

Within this spin–fluctuation scenario a simplified model of the pseudogap state was studied[2,4,5] under the assumption that the scattering by dynamic spin fluctuations can be reduced for high enough temperatures to a static Gaussian random field (quenched disorder) of pseudogap fluctuations. These fluctuations are defined by a characteristic scattering vector from the vicinity of $\mathbf{Q}$, with a width determined by the inverse correlation length of short–range order $\kappa = \xi^{-1}$.

Undoped cuprates are antiferromagnetic Mott insulators with $U \gg W$ (U — value of local Coulomb interaction, W — bandwidth of non–interacting band), so that correlation effects are very important. It is thus clear that the electronic properties of underdoped (and probably also optimally doped) cuprates are governed by strong electronic correlations too, so that these systems are typical strongly correlated metals. Two types of correlated metals can be distinguished: (i) the doped Mott insulator and (ii) the bandwidth controlled correlated metal $W \approx U$. Both types will be considered in this paper.

A state of the art tool to describe such correlated systems is the dynamical mean–field theory (DMFT)[6,7,8,9,10]. The characteristic features of correlated systems within the DMFT are the formation of incoherent structures, the so-called Hubbard bands, split by the Coulomb interaction U, and a quasiparticle (conduction) band near the Fermi level dynamically generated by the local correlations[6,7,8,9,10].

Unfortunately, the DMFT is not useful to the study the "antiferromagnetic" scenario of pseudogap formation in strongly correlated metals. This is due to the basic approximation of the DMFT, which amounts to the complete neglect of non-local dynamical correlation effects. The aim of the present paper is to formulate an approach overcoming this difficulty.

The paper is organized as follows: In section II we present a derivation of the self–consistent generalization we call DMFT+$\Sigma_{\mathbf{k}}$ which includes short-ranged dynamical correlations to some extent. Section III describes the construction of the $\mathbf{k}$–dependent self–energy, and some computational details are presented in section IV A. Results and a discussion are given in the sections IV and V.

II. INTRODUCING LENGTH SCALE INTO DMFT: DMFT+$\Sigma_{\mathbf{k}}$ APPROACH

Basic shortcoming of traditional DMFT approach[6,7,8,9,10] is the neglect of momentum dependence of electron self–energy. This approximation in principle allows for an exact solution of correlated electron systems fully preserving the local part of the dynamics introduced by electronic correlations. To include non–local effects, while remaining within the usual "impurity analogy", we propose the following procedure. To be definite, let us consider a standard one-band Hubbard model from now on. The extension to multi-orbital or multi-band models is straightforward. The major assumption of our approach is that the lattice and Matsubara "time" Fourier transform of the single-particle Green function can be written as:

$$G_{\mathbf{k}}(i\omega) = \frac{1}{i\omega + \mu - \varepsilon(\mathbf{k}) - \Sigma(i\omega) - \Sigma_{\mathbf{k}}(i\omega)}, \qquad \omega = \pi T(2n+1), \tag{1}$$

where $\Sigma(i\omega)$ is the *local* contribution to self–energy, surviving in the DMFT, while $\Sigma_{\mathbf{k}}(i\omega)$ is some momentum dependent part. We suppose that this last contribution is due to either electron interactions with some "additional" collective modes or order parameter fluctuations, or may be due to non–local contributions within the Hubbard model itself. The assumed additive form of self–energy $\Sigma(i\omega) + \Sigma_{\mathbf{k}}(i\omega)$ corresponds to neglect of possible interference of these local and non–local contributions.

The self–consistency equations of our generalized DMFT+$\Sigma_{\mathbf{k}}$ approach are formulated as follows:

1. Start with some initial guess of *local* self–energy $\Sigma(i\omega)$, e.g. $\Sigma(i\omega) = 0$.

2. Construct $\Sigma_{\mathbf{k}}(i\omega)$ within some (approximate) scheme, taking into account interactions with collective modes or order parameter fluctuations which in general can depend on $\Sigma(i\omega)$ and μ.

3. Calculate the local Green function

$$G_{ii}(i\omega) = \frac{1}{N}\sum_{\mathbf{k}} \frac{1}{i\omega + \mu - \varepsilon(\mathbf{k}) - \Sigma(i\omega) - \Sigma_{\mathbf{k}}(i\omega)}. \tag{2}$$

4. Define the "Weiss field"

$$\mathcal{G}_0^{-1}(i\omega) = \Sigma(i\omega) + G_{ii}^{-1}(i\omega). \tag{3}$$

5. Using some "impurity solver" to calculate the single-particle Green function for the effective Anderson impurity problem, defined by integral

$$G_d(\tau - \tau') = \frac{1}{Z_{\text{eff}}} \int Dc_{i\sigma}^{+} Dc_{i\sigma} c_{i\sigma}(\tau) c_{i\sigma}^{+}(\tau') \exp(-S_{\text{eff}}) \tag{4}$$

with effective action for a fixed site ("impurity") i

$$S_{\text{eff}} = -\int_0^\beta d\tau_1 \int_0^\beta d\tau_2 c_{i\sigma}(\tau_1) \mathcal{G}_0^{-1}(\tau_1 - \tau_2) c_{i\sigma}^{+}(\tau_2) + \int_0^\beta d\tau U n_{i\uparrow}(\tau) n_{i\downarrow}(\tau) \quad , \tag{5}$$

$Z_{\text{eff}} = \int Dc_{i\sigma}^{+} Dc_{i\sigma} \exp(-S_{\text{eff}})$, and $\beta = T^{-1}$. This step produces a *new* set of values $G_d^{-1}(i\omega)$.

6. Define a *new* local self–energy

$$\Sigma(i\omega) = \mathcal{G}_0^{-1}(i\omega) - G_d^{-1}(i\omega). \tag{6}$$

7. Using this self–energy as "initial" one in step 1, continue the procedure until (and if) convergency is reached to obtain

$$G_{ii}(i\omega) = G_d(i\omega). \tag{7}$$

Eventually, we get the desired Green function in the form of (1), where $\Sigma(i\omega)$ and $\Sigma_{\mathbf{k}}(i\omega)$ are those appearing at the end of our iteration procedure. A more detailed derivation of this scheme within a diagrammatic approach is given in the Appendix A.

III. CONSTRUCTION OF K–DEPENDENT SELF–ENERGY

For the momentum dependent part of the single-particle self–energy we concentrate on the effects of scattering of electrons from collective short-range SDW–like antiferromagnetic spin (or CDW–like charge) fluctuations. To calculate $\Sigma_{\mathbf{k}}(i\omega)$ for an electron moving in the quenched random field of (static) Gaussian spin (or charge) fluctuations with dominant scattering momentum transfers from the vicinity of some characteristic vector $\mathbf{Q}$, we use a slightly generalized version of the recursion procedure proposed in Refs.[4,5,11] and take into account *all* Feynman diagrams describing the scattering of electrons by this random field. Then the desired self–energy is given by

$$\Sigma_{\mathbf{k}}(i\omega) = \Sigma_{n=1}(i\omega\mathbf{k}) \tag{8}$$

with

$$\Sigma_n(i\omega\mathbf{k}) = \Delta^2 \frac{s(n)}{i\omega + \mu - \Sigma(i\omega) - \varepsilon_n(\mathbf{k}) + inv_n\kappa - \Sigma_{n+1}(i\omega\mathbf{k})} \quad . \tag{9}$$

The quantity Δ characterizes the energy scale and $\kappa = \xi^{-1}$ is the inverse correlation length of short range SDW (CDW) fluctuations, $\varepsilon_n(\mathbf{k}) = \varepsilon(\mathbf{k}+\mathbf{Q})$ and $v_n = |v^x_{\mathbf{k}+\mathbf{Q}}| + |v^y_{\mathbf{k}+\mathbf{Q}}|$ for odd n while $\varepsilon_n(\mathbf{k}) = \varepsilon(\mathbf{k})$ and $v_n = |v^x_{\mathbf{k}}| + |v^y_{\mathbf{k}}|$ for even n. The velocity projections $v^x_{\mathbf{k}}$ and $v^y_{\mathbf{k}}$ are determined by usual momentum derivatives of the "bare" electronic energy dispersion $\varepsilon(\mathbf{k})$. Finally, $s(n)$ represents a combinatorial factor with

$$s(n) = n \tag{10}$$

for the case of commensurate charge (CDW type) fluctuations with $\mathbf{Q} = (\pi/a, \pi/a)$[11]. For incommensurate CDW fluctuations[11] one finds

$$s(n) = \begin{cases} \frac{n+1}{2} & \text{for odd } n \\ \frac{n}{2} & \text{for even } n. \end{cases} \tag{11}$$

If we want to take into account the (Heisenberg) spin structure of interaction with spin fluctuations in "nearly antiferromagnetic Fermi–liquid" (spin–fermion (SF) model Ref.[4]), the combinatorics of diagrams becomes more complicated. Spin–conserving scattering processes obey commensurate combinatorics, while spin–flip scattering is described by diagrams of incommensurate type ("charged" random field in terms of Ref.[4]). In this model the recursion relation for the single-particle Green function is again given by (9), but the combinatorial

factor $s(n)$ now acquires the following form[4]:

$$s(n) = \begin{cases} \frac{n+2}{3} & \text{for odd } n \\ \frac{n}{3} & \text{for even } n. \end{cases} \tag{12}$$

Obviously, with this procedure we introduce an important length scale ξ not present in standard DMFT. Physically this scale mimics the effect of short-range (SDW or CDW) correlations within fermionic "bath" surrounding the effective Anderson of the DMFT impurity. We expect that such a length-scale will lead to a competition between local and non-local physics.

An important aspect of the theory is that both parameters Δ and ξ can in principle be calculated from the microscopic model at hand. For example, using the two–particle selfconsistent approach of Ref.[12] with the approximations introduced in Refs.[4,5], one can derive within the standard Hubbard model the following microscopic expression for Δ:

$$\begin{aligned} \Delta^2 = \frac{1}{4}U^2 \frac{< n_{i\uparrow} n_{i\downarrow} >}{< n_{i\uparrow} >< n_{i\downarrow} >} [< n_{i\uparrow} > + < n_{i\downarrow} > -2 < n_{i\uparrow} n_{i\downarrow} >] = \\ = U^2 \frac{< n_{i\uparrow} n_{i\downarrow} >}{n^2} < (n_{i\uparrow} - n_{i\downarrow})^2 >= \\ = U^2 \frac{< n_{i\uparrow} n_{i\downarrow} >}{n^2} \frac{1}{3} < \mathbf{S}_i^2 >, \end{aligned} \tag{13}$$

where we consider only scattering from antiferromagnetic spin fluctuations. The different local quantities – spin fluctuation $< \mathbf{S}_i^2 >$, density n and double occupancy $< n_{i\uparrow} n_{i\downarrow} >$ – can easily be calculated within the standard DMFT[9]. A detailed derivation of (13) and computational results for Δ obtained by DMFT using quantum Monte–Carlo (QMC) to solve the effective impurity problem are presented in Appendix B. A corresponding microscopic expressions for the correlation length $\xi = \kappa^{-1}$ can also be derived within the two–particle self–consistent approach[12]. However, we expect those results for ξ to be less reliable, because this approach is valid only for relatively small (or medium) values of U/t. Thus, in the following we will consider both Δ and especially ξ as some phenomenological parameters to be determined from experiments.

IV. RESULTS AND DISCUSSION

A. Computation details

In the following, we want to discuss results for a standard one-band Hubbard model on a square lattice. With nearest (t) and next nearest (t') neighbour hopping integrals the dispersion then reads

$$\varepsilon(\mathbf{k}) = -2t(\cos k_x a + \cos k_y a) - 4t' \cos k_x a \cos k_y a \ , \tag{14}$$

where a is the lattice constant. The correlations are introduced by a repulsive local two-particle interaction U. We choose as energy scale the nearest neighbour hopping integral t and as length scale the lattice constant a.

For a square lattice the bare bandwidth is $W = 8t$. To study a strongly correlated metallic state obtained as doped Mott insulator we use $U = 40t$ as value for the Coulomb interaction and a filling $n = 0.8$ (hole doping). The correlated metal in the case of $W \gtrsim U$ is realized via $U = 4t$ and two fillings: half–filling ($n = 1.0$) and $n = 0.8$ (hole doping). As typical values for Δ we choose $\Delta = t$ and $\Delta = 2t$ (actually as approximate limiting values — cf. Appendix B) and for the correlation length $\xi = 2a$ and $\xi = 10a$ (motivated mainly by experimental data for cuprates[2,4]).

The DMFT maps the lattice problem onto an effective, self–consistent impurity defined by Eqs. (4)-(5). In our work we employ as "impurity solvers" two reliable numerically exact methods — quantum Monte–Carlo (QMC)[13] and numerical renormalization group (NRG)[15,16]. Calculations were done for the case $t' = 0$ and t'/t=-0.4 (more or less typical for cuprates) at two different temperatures $T = 0.088t$ and $T = 0.356t$ (for NRG computations)[21] . QMC computations of double occupancies as functions of filling were done at temperatures $T = 0.1t$ and $T = 0.4t$ [22].

B. Generalized DMFT+$\Sigma_{\mathbf{k}}$ approach: densities of states

Let us start the discussion of our results obtained within our generalized DMFT+$\Sigma_{\mathbf{k}}$ approach with the densities of states (DOSs) for the case of small (relative to bandwidth) Coulomb interaction $U = 4t$ with and without pseudogap fluctuations. As already discussed in the introduction, the characteristic feature of the strongly correlated metallic state is the

coexistence of lower and upper Hubbard bands split by the value of U with a quasiparticle peak at the Fermi level. Since at half–filling the bare DOS of the square lattice has a Van–Hove singularity at the Fermi level ($t' = 0$) or close to it (in case of $t'/t = -0.4$) one cannot treat a peak on the Fermi level simply as a quasiparticle peak. In fact, there are two contributions to this peak from (i) the quasiparticle peak appearing in strongly correlated metals due to many-body effects and (ii) the smoothed Van–Hove singularity from the bare DOS[17]. In Figs. 1 and 2 we show the corresponding DMFT(NRG) DOSs without pseudogap fluctuations as black lines for $n = 1$ and $n = 0.8$ for both bare dispersions $t'/t = -0.4$ (left panels) and for $t' = 0$ (right panels) for two different temperatures $T = 0.356t$ (middle panels) and $T = 0.088t$ (upper and lower panels). The remaining curves in Figs. 1 and 2 represent results for the DOSs with non-local fluctuations switched on. The fluctuation amplitudes are taken as $\Delta = 2t$ (upper and and middle panels) and $\Delta = t$ (low panels). For all sets of parameters one can see that the introduction of non-local fluctuations into the calculation leads to the formation of pseudogap in the quasiparticle peak.

The behaviour of the pseudogaps in the DOSs has some common features. For example, for t'=0 at half–filling (Fig. 1, right column) we find that the pseudogap is most pronounced. For $n = 0.8$ (Fig. 2, right column) the picture is almost the same but slightly asymmetric. The width of the pseudogap (the distance between peaks closest to Fermi level) appears to be of the order of $\sim 2\Delta$ here. Decreasing the value of Δ from $2t$ to t leads to a pseugogap that is correspondingly twice smaller and in addition more shallow. When one uses the combinatorial factors corresponding to the spin–fermion model (Eq.(12)), we find that the pseudogap becomes more pronounced than in the case of commensurate charge fluctuations (combinatorial factors of Eq. (11)). The influence of the correlation length ξ can be seen is also as expected. Changing ξ^{-1} from $\xi^{-1} = 0.1$ to $\xi^{-1} = 0.5$, i.e. decreasing the range of the non-local fluctuations, slightly washes out the pseudogap. Also, increasing the temperature from $T = 0.088t$ to $T = 0.356t$ leads to a general broadening of the structures in the DOSs. These observations remain at least qualitatively valid for $t'/t = -0.4$ (Figs. 1 and 2, left columns) with an additional asymmetry due to the next-nearest neighbour hopping. Noteworthy is however the fact that for $t'/t = -0.4$ and $\xi^{-1} = 0.5$ the pseudogap has almost disappeared for the temperatures studied here. An also very remarkable point is the similarity of the results obtained with the generalized DMFT+$\Sigma_{\mathbf{k}}$ approach with $U = 4t$ (smaller than the bandwidth W) to those obtained earlier without Hubbard–like Coulomb

interactions[4,5].

Let us now consider the case of a doped Mott insulator. The model parameters are again $t' = 0$ and $t'/t = -0.4$ with filling $n = 0.8$, but the Coulomb interaction strength is set to $U = 40t$ for our DMFT+$\Sigma_{\mathbf{k}}$ calculations. Characteristic features of the DOS for such a strongly correlated metal are a strong separation of lower and upper Hubbard bands and a Fermi level crossing by the lower Hubbard band (for non–half–filled case). Without non-local fluctuations the quasi-particle peak is again formed at the Fermi level; but now the upper Hubbard band is far to the right and does not touch the quasiparticle peak (as it was for the case of small Coulomb interactions). DOSs without non-local fluctuations are again presented as black lines on Fig. 4 ($t' = 0$) and Fig. 3 ($t'/t = -0.4$).

With rather strong non-local fluctuations $\Delta = 2t$, a pseudogap appears in the middle of quasiparticle peak. In addition we observe that the lower Hubbard band is slightly broadened by fluctuation effects. Qualitative behaviour of the pseudogap anomalies is again similar to those described above for the case of $U = 4t$, e.g. a decrease of ξ makes the pseudogap less pronounced, reducing Δ from $\Delta = 2t$ to $\Delta = t$ narrows of the pseudogap and also makes it more shallow etc.. Note that for the doped Mott–insulator we find that the pseudogap is remarkably more pronounced for the SDW–like fluctuations than for CDW–like fluctuations.

There are, however, quite clear differences to the case with $U = 4t$. For example, the width of the pseudogap appears to be much smaller than 2Δ, which we attribute to the fact that the quasiparticle peak itself is actually rather narrow now.

C. Generalized DMFT+$\Sigma_{\mathbf{k}}$ approach: spectral functions $A(\omega, \mathbf{k})$

In the previous subsections we discussed the densities of states obtained self–consistently by the DMFT+$\Sigma_{\mathbf{k}}$ approach. Once we get a self–consistent solution of the DMFT+$\Sigma_{\mathbf{k}}$ equations with non-local fluctuations we can of course also compute the spectral functions $A(\omega, \mathbf{k})$

$$A(\omega, \mathbf{k}) = -\frac{1}{\pi}\mathrm{Im}\frac{1}{\omega + \mu - \varepsilon(\mathbf{k}) - \Sigma(\omega) - \Sigma_{\mathbf{k}}(\omega)}, \tag{15}$$

where self–energy $\Sigma(\omega)$ and chemical potential μ are calculated self–consistently as described in Sec. II. To plot $A(\omega, \mathbf{k})$ we choose $\mathbf{k}$–points along the "bare" Fermi surfaces for different types of lattice spectra and fillings. In Fig. 5 one can see corresponding shapes of these "bare" Fermi surfaces (presented are only 1/8-th parts of the Fermi surfaces within the first

quadrant of the Brillouin zone).

In the following we concentrate mainly on the case $U = 4t$ and filling $n = 0.8$ (Fermi surface of Fig. 5(a)). The corresponding spectral functions $A(\omega, \mathbf{k})$ are depicted in Fig. 7. When $t'/t = -0.4$ (upper row), the spectral function close to the Brillouin zone diagonal (point B) has the typical Fermi–liquid behaviour, consisting of a rather sharp peak close to the Fermi level. In the case of SDW–like fluctuations this peak is shifted down in energy by about $-0.5t$ (left upper corner). In the vicinity of the "hot–spot" the shape of $A(\omega, \mathbf{k})$ is completely modified. Now $A(\omega, \mathbf{k})$ becomes double–peaked and non–Fermi–liquid–like. Directly at the "hot–spot", $A(\omega, \mathbf{k})$ for SDW–like fluctuations has two equally intensive peaks situated symmetrically around the Fermi level and split from each other by $\sim 1.5\Delta$ Refs.[4,5]. For commensurate CDW–like fluctuations the spectral function in the "hot–spot" region has one broad peak centred at the Fermi level with width $\sim \Delta$. Such a merging of the two peaks at the "hot–spot" for commensurate fluctuations was previously observed in Ref.[5]. However close to point A this type of fluctuations also produces a double–peak structure in the spectral function.

In Fig. 6 we show spectral functions for the case of $U = 4t$ at half–filling ($n = 1$) (Fermi surface of Fig. 5 (c), (d)). For $t'/t = -0.4$ (upper row of Fig. 6) these are similar to those just discussed for $n = 0.8$. However, the pseugogap is more pronounced here and remains open even close to the antiferromagnetic Fermi surface boundary (point B) for SDW fluctuations.

In the lower panel of Fig. 7 we show spectral functions for 20% hole doping ($n = 0.8$) and the case of $t' = 0$ (Fermi surface from Fig. 5(b)). Since the Fermi surface now is close to the antiferromagnetic zone boundary, the pseudogap anomalies are rather strong and almost non–dispersive along the Fermi surface. At half–filling (Fig. 7, lower panel) and for $t' = 0$ the Fermi surface (Fig. 5(d)) actually coincides with antiferromagnetic zone boundary. In this case the the whole Fermi surface is the "hot–region" (perfect "nesting"). The spectral functions are now symmetric around the Fermi level. For SDW–like fluctuations there are two peaks split by $\sim 1.5\Delta$. Again, CDW–like fluctuations give just one peak centred at the Fermi level with width $\sim \Delta$.

For the case of a doped Mott insulator ($U = 40t$, $n = 0.8$), the spectral functions obtained by the DMFT+$\Sigma_{\mathbf{k}}$ approach are presented in Fig. 8. Qualitatively, the shapes of these spectral functions are similar to those shown on Fig. 7. As was pointed out above, the strong

Coulomb correlations lead to a narrowing of the quasiparticle peak and a corresponding decrease of the pseudogap width. One should also note that in contrast to $U = 4t$ the spectral functions are now less intensive, because part of the spectral weight is transferred to the upper Hubbard band located at about $40t$.

Using another quite common choice of $\mathbf{k}$–points we can compute $A(\omega, \mathbf{k})$ along high–symmetry directions in the first Brillouin zone: $\Gamma(0,0) - \mathrm{X}(\pi,0) - \mathrm{M}(\pi,\pi) - \Gamma(0,0)$. The spectral functions for these $\mathbf{k}$–points are colelcted in Figs. 9, 10 and 11 for the case of SDW–like fluctuations. For all sets of parameters one can see a characteristic double peak pseudogap structure at the X point and in the middle of $M-\Gamma$ direction. A change of the filling leads mainly to a rigid shift of spectral functions with respect to the Fermi level.

With the spectral functions we are now of course in a position to calculate angle resolved photoemission spectra (ARPES), which is the most direct experimental way to observe pseudogap in real compounds. For that purpose, we only need to multiply our results for the spectral functions with the Fermi function at temperature $T = 0.088t$. the resulting DMFT+$\Sigma_{\mathbf{k}}$ ARPES spectra are presented in Figs. 12, 13 and 14 One should note that for $t'/t = -0.4$ (upper panel of Figs. 12, 13 and 14) as $\mathbf{k}$ goes from point "A" to point "B" the peak situated slightly below the Fermi level changes its position and moves down in energy. Simultaneously it becomes more broad and less intensive. The dotted line guides the motion of the peak maximum. Also at the "hot–spot" and further to point B one can see some signs of the double–peak structure. Such behaviour of the peak in the ARPES is rather reminiscent of those observed experimentally in underdoped cuprates[2,4,18].

V. CONCLUSION

To summarize, we propose a generalized DMFT+$\Sigma_{\mathbf{k}}$ approach, which is meant to take into account the important effects due to non–local correlations in a systematic, but to some extent phenomenological fashion. The main idea of this extension is to stay within a usual effective Anderson impurity analogy, and introducing length scales due to non-local correlation via the effective medium ("bath") appearing in the standard DMFT. This becomes possible by incorporating scattering processes of fermions in the "bath" from non-local collective SDW–like antiferromagnetic spin (or CDW–like charge) fluctuations. Such a generalization of the DMFT allows one to overcome the well–known shortcoming of $\mathbf{k}$–

independence of self–energy of standard DMFT. It in turn opens the possibility to access the physics of low–dimensional strongly correlated systems, where different types of spatial fluctuations (e.g. of some order parameter), become important in a non-perturbative way at least with respect to the important local dynamical correlations. However, we must stress that our procedure in no way introduces any kind of systematic $1/d$–expansion, being only a qualitative method to include length scale into DMFT.

In our present study we addressed the problem of pseudogap formation in the strongly correlated metallic state. We showed evidence that the pseudogap appears at the Fermi level within the quasiparticle peak, introducing a new small energy scale of the order of Δ in the DOSs and spectral functions $A(\omega, \mathbf{k})$.

Let us stress, that our generalization of DMFT leads to non–trivial and in our opinion physically sensible $\mathbf{k}$–dependence of spectral functions. In contrast, in a recent work by Haule *et al.*[19] the extended DMFT approach was used to demonstrate pseudogap formation in DOS due to dynamic Coulomb correlations only. However, within the approach of Ref.[19] there is no way to obtain $\mathbf{k}$–dependence of spectral functions beyond that originating from the bare electronic energy dispersion which is actually observed in experiments. Of course, similar results and observations were in recent years also made using the cluster mean-field theories[20]. The major advantage of our approach over these cluster mean-field theories is, that we stay in an effective single-impurity picture. This means that our approach is computationally much less expensive and therefore also easily generalizable to multi-orbital systems.

VI. ACKNOWLEDGEMENTS

We are grateful to A. Kampf for useful discussions. This work was supported in part by RFBR grants 05-02-16301 (MS,EK,IN) RFFI-GFEN-03-02-39024_a (VA,IN), RFFI-04-02-16096 (VA,IN), by the joint UrO-SO project *No.* 22 (VA,IN), and programs of the Presidium of the Russian Academy of Sciences (RAS) "Quantum macrophysics" and of the Division of Physical Sciences of the RAS "Strongly correlated electrons in semiconductors, metals, superconductors and magnetic materials". I.N. acknowledges support from the Dynasty Foundation and International Centre for Fundamental Physics in Moscow program for young scientists 2005), Russian Science Support Foundation program for young PhD of Russian

Academy of Science 2005. One of us (TP) further acknowledges supercomputer support from the Norddeutsche Verbund für Hoch- und Höchstleistungsrechnen.

APPENDIX A: DERIVATION OF GENERALIZED DMFT+$\Sigma_{\mathbf{k}}$ APPROACH

In this appendix we present a derivation of the generalized DMFT+$\Sigma_{\mathbf{k}}$ scheme for the Hubbard model

$$H = -\sum_{ij,\sigma} t_{ij} c^{\dagger}_{i\sigma} c_{j\sigma} + U \sum_{i} n_{i\uparrow} n_{i\downarrow}, \tag{A1}$$

using a diagrammatic approach. The single–particle Green function in Matsubara representation is as usual given by

$$G_{\mathbf{k}}(i\omega) = \frac{1}{i\omega + \mu - \varepsilon(\mathbf{k}) - \Sigma(i\omega, \mathbf{k})} \tag{A2}$$

To establish the standard DMFT one invokes the limit of infinite dimensions $d \to \infty$. In this limit only local contributions to electron self–energy survive[7,9], i.e. $\Sigma_{ij} \to \delta_{ij}\Sigma_{ii}$ or, in reciprocal space, $\Sigma(i\omega, \mathbf{k}) \to \Sigma(i\omega)$.

In Fig. 15 we show examples of "skeleton" diagrams for the local self – energy, contributing in the limit of $d \to \infty$. The complete series of these and similar diagrams defines the local self – energy as a functional of the local Green function

$$\Sigma = F[G_{ii}] \ , \tag{A3}$$

where

$$G_{ii}(i\omega) = \frac{1}{N} \sum_{\mathbf{k}} \frac{1}{i\omega + \mu - \varepsilon(\mathbf{k}) - \Sigma(i\omega)}. \tag{A4}$$

One then defines the "Weiss field"

$$\mathcal{G}_0^{-1}(i\omega) = \Sigma(i\omega) + G_{ii}^{-1}(i\omega) \tag{A5}$$

which is used to set up the effective impurity problem with an effective action given by (5). Via Dyson's equation the Green function (4) for this effective impurity problem can be written as

$$G_d(i\omega) = \frac{1}{\mathcal{G}_0^{-1}(i\omega) - \Sigma_d(i\omega)} \tag{A6}$$

and the "skeleton" diagrams for self–energy Σ_d are just the same as shown in Fig. 15, with the replacement $G_{ii} \to G_d$. Thus we get

$$\Sigma_d = F[G_d], \tag{A7}$$

where F is the same functional as in (A3). The two equations (A6) and (A7) define both G_d and Σ_d for a given "Weiss field" $\mathcal{G}_0$. On the other hand, for the local Σ and G_{ii} of the

initial (Hubbard) problem we have precisely the same pair of equations, viz (A3) and (A5), and $\mathcal{G}_0$ in both problems is just the same, so that

$$\Sigma = \Sigma_d; \qquad G_{ii} = G_d. \tag{A8}$$

Thus, the task of finding the local self–energy of the ($d \to \infty$) Hubbard model is eventually reduced to the calculation of the self–energy of an effective quantum impurity problem defined by effective action of Eq. (5).

Consider now non – local contribution to the self – energy. If we neglect interference between local and non–local contributions (as given e.g. by the diagram shown in Fig.16(b)), the full self–energy is approximately determined by the sum of these two contributions. "Skeleton" diagrams for the non-local part of the self–energy, $\Sigma_{\mathbf{k}}(i\omega)$, are then those shown in Fig. 16(a), where the full line denotes the Green function $G_{\mathbf{k}}$ of Eq. (1), while broken lines denote the interaction with static Gaussian spin (charge) fluctuations.

The local contribution to the self–energy is again defined by the functional (A3) via the local Green function G_{ii}, which is now given by (2). Introducing again a "Weiss field" via (A5) and repeating all previous arguments, we again reduce the task of finding the local part of the self–energy to the solution of an "impurity" problem with an effective action (5).

To determine the non–local contribution $\Sigma_{\mathbf{k}}(i\omega)$ we first introduce

$$\mathcal{G}_{0\mathbf{k}}(i\omega) = \frac{1}{G^{-1}_{\mathbf{k}}(i\omega) + \Sigma_{\mathbf{k}}(i\omega)} = \frac{1}{i\omega + \mu - \varepsilon(\mathbf{k}) - \Sigma(i\omega)} \tag{A9}$$

as the "bare" Green function for electron scattering by static Gaussian spin (charge) fluctuations. The assumed static nature of these fluctuations allows to use the method of Refs.[4,5,11] and the calculation of the non–local part of the self–energy $\Sigma_{\mathbf{k}}(i\omega)$ reduces to the recursion procedure defined by Eqs. (8) and (9). The choice of the "bare" Green function Eq. (A9) guarantees that the Green function "dressed" by fluctuations $G^{-1}_{\mathbf{k}}(i\omega) = \mathcal{G}^{-1}_{0\mathbf{k}}(i\omega) - \Sigma_{\mathbf{k}}(i\omega)$, which enters into the "skeleton" diagrams for $\Sigma_{\mathbf{k}}(i\omega)$, just coincides with the full Green functions $G_{\mathbf{k}}(i\omega)$.

Thus we obtain a fully self–consistent scheme to calculate both local (due to strong single–site correlations) and non–local (due to short–range fluctuations) contributions to electron self–energy.

APPENDIX B: Δ IN THE HUBBARD MODEL.

In this Appendix we derive the explicit microscopic expression for pseudogap amplitude Δ given in (13). Within the two–particle self–consistent approach of Ref.[12], valid for medium values of U, and neglecting charge fluctuations, we can write down an expression for the electron self–energy of the form used in (1), with

$$\Sigma_\sigma(i\omega) = U n_{-\sigma} \tag{B1}$$

as the lowest order local contribution due to the on–site Hubbard interaction, surviving in the limit of $d \to \infty$, and exactly accounted for in DMFT (with all higher–order contributions). Non–local contribution to the self–energy (vanishing for $d \to \infty$) due to interaction with spin–fluctuations then lead to the expression

$$\Sigma_{\mathbf{k}}(i\omega) = \frac{U}{4}\frac{T}{N}\sum_m \sum_{\mathbf{q}} U_{sp}\chi_{sp}(\mathbf{q},\nu_m) G_0(\mathbf{k}+\mathbf{q}, i\omega + i\nu_m)\ , \tag{B2}$$

where

$$U_{sp} = g_{\uparrow\downarrow}(0)U, \qquad g_{\uparrow\downarrow}(0) = \frac{< n_{i\uparrow} n_{i\downarrow} >}{< n_{i\uparrow} >< n_{i\downarrow} >} \tag{B3}$$

with $< n_\sigma^2 >=< n_\sigma >$ and $< n_{i\uparrow} >=< n_{i\downarrow} >= \frac{1}{2}n$ in the paramagnetic phase. For the dynamic spin susceptibility $\chi_{sp}(\mathbf{q},\nu_m)$ we use the standard Ornstein–Zernike form[12], similar to that used in spin–fermion model[4], which describes enhanced scattering with momenta transfer close to antiferromagnetic vector $\mathbf{Q} = (\pi/a, \pi/a)$. With these approximations, we can write down the following expression for the non–local contribution to the self–energy[4,5]:

$$\begin{aligned}
\Sigma_{\mathbf{k}}(i\omega) &= \frac{1}{4}UU_{sp}\frac{T}{N}\sum_m\sum_{\mathbf{q}}\chi_{sp}(\mathbf{q},\nu_m)\frac{1}{i\omega + i\nu_m + \mu - \varepsilon(\mathbf{k}+\mathbf{q})} \approx \\
&\approx \frac{1}{4}UU_{sp}\frac{T}{N}\sum_m\sum_{\mathbf{q}}\chi_{sp}(\mathbf{q},\nu_m)\sum_{\mathbf{q}} S(\mathbf{q})\frac{1}{i\omega + \mu - \varepsilon(\mathbf{k}+\mathbf{q})} \equiv \\
&\equiv \Delta^2 \sum_{\mathbf{q}} S(\mathbf{q})\frac{1}{i\omega + \mu - \varepsilon(\mathbf{k}+\mathbf{q})} = \\
&= \frac{\Delta^2}{i\omega + \mu - \varepsilon(\mathbf{p}+\mathbf{Q}) + i(|v^x_{\mathbf{p}+\mathbf{Q}}| + |v^y_{\mathbf{p}+\mathbf{Q}}|)\kappa \mathrm{sign}\omega}.
\end{aligned} \tag{B4}$$

Here we have introduced the static form factor[5]

$$S(\mathbf{q}) = \frac{2\xi^{-1}}{(q_x - Q_x)^2 + \xi^{-2}}\frac{2\xi^{-1}}{(q_y - Q_y)^2 + \xi^{-2}} \tag{B5}$$

and the squared pseudogap amplitude

$$\Delta^2 = \frac{1}{4} U U_{sp} \frac{T}{N} \sum_m \sum_{\mathbf{q}} \chi_{sp}(\mathbf{q}, \nu_m) =$$

$$= \frac{1}{4} U U_{sp} [< n_{i\uparrow} > + < n_{i\downarrow} > -2 < n_{i\uparrow} n_{i\downarrow} >] =$$

$$= \frac{1}{4} U U_{sp} \frac{1}{3} < \mathbf{S}_i^2 >, \tag{B6}$$

where we have used the exact sum–rule for the susceptibility[4,12]. Taking into account (B3) we immediately obtain (13).

Actually, the approximations made in (B4) and (B5) allow for an exact summation of the whole Feynman series for electron interaction with spin–fluctuations, replaced by the static Gaussian random field. Thus generalizing the one–loop approximation (B4) eventually leads to the basic recursion procedure given in (8), (9) Refs.[4,5].

Using the DMFT(QMC) approach we computed occupancies $< n_{i\uparrow} >$, $< n_{i\downarrow} >$ and double occupancies $< n_{i\uparrow} n_{i\downarrow} >$ required to calculate the pseudogap amplitude Δ of Eq. (B6) In Fig. 17 the corresponding values of Δ are presented. One can see that Δ grows when the filling goes to $n = 1$. While U approaches $8t$ (the value of the bandwidth for a square lattice) Δ as a function of n grows monotonically. When U becomes larger than $W = 8t$ (when a metal–insulator transition occurs) one can see a local minimum for $n = 0.9$, which becomes more pronounced with further increase of U. For $t'/t = -0.4$ and both temperatures the scatter of Δ values is smaller than for the case of $t' = 0$. Also Δ has a rather weak temperature dependence. All values of Δ lie in the interval $\sim 0.75t \div 2t$. Therefore, for our computations we took only two characteristic values of $\Delta = t$ and $\Delta = 2t$.

[1] T. Timusk, B. Statt, Rep. Progr. Phys, **62**, 61 (1999).

[2] M. V. Sadovskii, Usp. Fiz. Nauk **171**, 539 (2001) [Physics – Uspekhi **44**, 515 (2001)].

[3] D. Pines, ArXiv: cond-mat/0404151.

[4] J. Schmalian, D. Pines, B.Stojkovic, Phys. Rev. B **60**, 667 (1999).

[5] E. Z. Kuchinskii, M. V. Sadovskii, Zh. Eksp. Teor. Fiz. **115**, 1765 (1999) [(JETP **88**, 347 (1999)].

[6] W. Metzner and D. Vollhardt, Phys. Rev. Lett. **62**, 324 (1989).

[7] D. Vollhardt, in *Correlated Electron Systems*, edited by V. J. Emery, World Scientific, Singapore, 1993, p. 57.

[8] Th. Pruschke, M. Jarrell, and J. K. Freericks, Adv. in Phys. **44**, 187 (1995).

[9] A. Georges, G. Kotliar, W. Krauth, and M. J. Rozenberg, Rev. Mod. Phys. **68**, 13 (1996).

[10] G. Kotliar and D. Vollhardt, Physics Today **57**, No. 3 (March), 53 (2004).

[11] M. V. Sadovskii, Zh. Eksp. Teor. Fiz. **77**, 2070(1979) [Sov.Phys.–JETP **50**, 989 (1979)].

[12] Y. M. Vilk, A.-M. S. Tremblay, J. Phys. I France **7**, 1309 (1997).

[13] J. E. Hirsch and R. M. Fye, Phys. Rev. Lett. **56**, 2521 (1986); M. Jarrell, Phys. Rev. Lett. **69**, 168 (1992); M. Rozenberg, X. Y. Zhang, and G. Kotliar, Phys. Rev. Lett. **69**, 1236 (1992); A. Georges and W. Krauth, Phys. Rev. Lett. **69**, 1240 (1992); M. Jarrell in *Numerical Methods for lattice Quantum Many-Body Problems*, edited by D. Scalapino, Addison Wesley, 1997. For review of QMC for DMFT see Ref.[14].

[14] K. Held, I.A. Nekrasov, N. Blümer, V.I. Anisimov, and D. Vollhardt, Int. J. Mod. Phys. B **15**, 2611 (2001); K. Held, I.A. Nekrasov, G. Keller, V. Eyert, N. Blümer, A.K. McMahan, R.T. Scalettar, T. Pruschke, V.I. Anisimov, and D. Vollhardt, cond-mat/0112079 (Published in *Quantum Simulations of Complex Many-Body Systems: From Theory to Algorithms*, eds. J. Grotendorst, D. Marks, and A. Muramatsu, NIC Series Volume 10 (NIC Directors, Forschunszentrum Jülich, 2002) p. 175-209.

[15] K.G. Wilson, Rev. Mod. Phys. **47**, 773 (1975); H.R. Krishna-murthy, J.W. Wilkins, and K.G. Wilson, Phys. Rev. B **21**, 1003 (1980); *ibid.* **21**, 1044 (1980); for a comprehensive introduction to teh NRG see e.g. A.C. Hewson, *The Kondo Problem to Heavy Fermions* (Cambridge University Press, 1993).

[16] R. Bulla, A.C. Hewson and Th. Pruschke, J. Phys. – Condens. Matter **10**, 8365(1998); R. Bulla, Phys. Rev. Lett. **83**, 136 (1999).

[17] We have checked that with increasing of Coulomb repulsion the Van–Hove singularity transforms gradiently into quasiparticle peak for $U = (6 \div 8)t$.

[18] A. Kaminski, H. M. Fretwell, M. R. Norman, M. Randeria, S. Rosenkranz, U. Chatterjee, J. C. Campuzano, J. Mesot, T. Sato, T. Takahashi, T. Terashima, M. Takano, K. Kadowaki, Z. Z. Li, H. Raffy, Phys. Rev. B **71**, 014517 (2005).

[19] K. Haule, A. Rosch, J. Kroha, P. Wölfle, Phys. Rev. B **68**, 155119 (2003).

[20] Th. Maier, M. Jarrell, Th. Pruschke and M. Hettler, Rev. Mod. Phys. (in print, cond-mat/0404055 (2004)).

[21] Discretization parameter Λ=2, number of low energy states after truncation 1000, cut-off near Fermi energy 10^{-6}, broadening parameter b=0.6.

[22] Number warm-up sweeps 30000, number of QMC sweeps 200000, number of imaginary time slices 40.

FIGURES

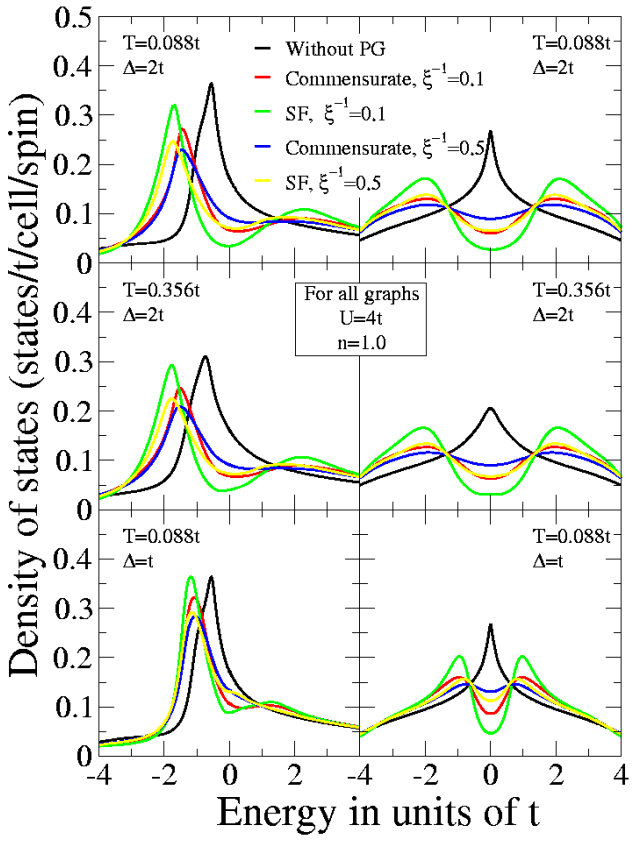

FIG. 1: Comparison of DOSs obtained from DMFT(NRG)+$\Sigma_{\mathbf{k}}$ calculations for different combinatorical factors (SF — spin–fermion model, commensurate), inverse correlation lengths (ξ^{-1}) in units of the lattice constant, temperatures (T) and values of the pseudogap potential (Δ). Left column corresponds to $t'/t = -0.4$, right column to $t' = 0$. In all graphs the Coulomb interaction is $U = 4t$ and $n = 1$. The Fermi level corresponds to zero.

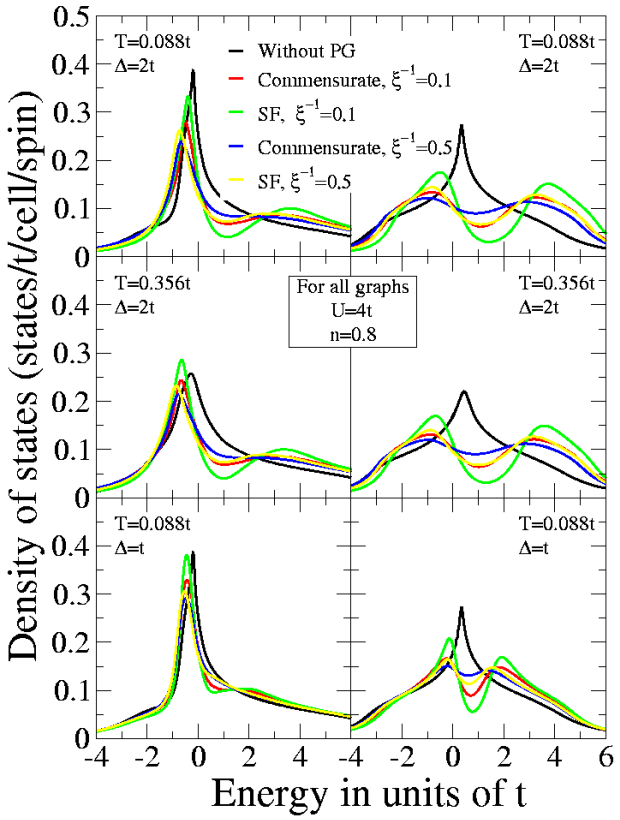

FIG. 2: Comparison of DOSs obtained from DMFT(NRG)+$\Sigma_{\mathbf{k}}$ calculations for a filling $n = 0.8$, other parameters as in Fig. 1.

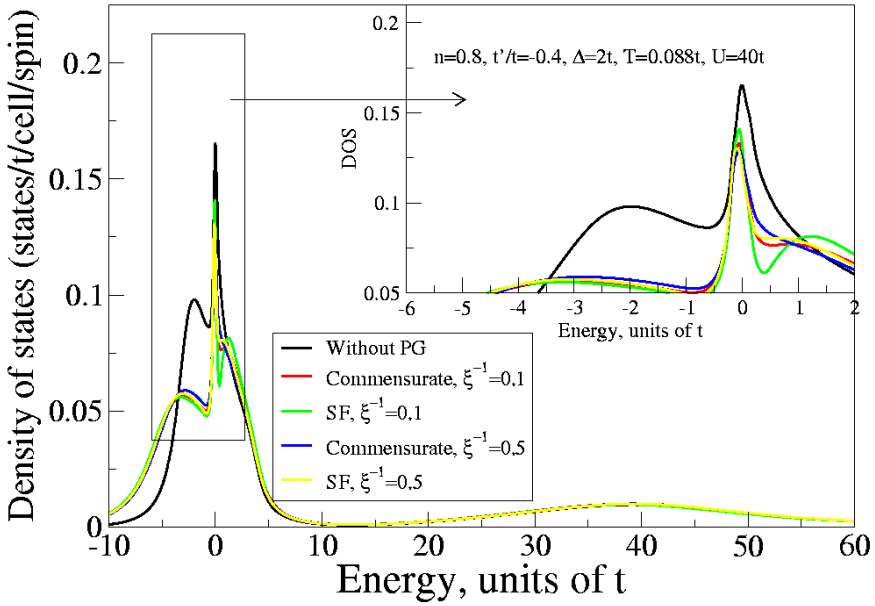

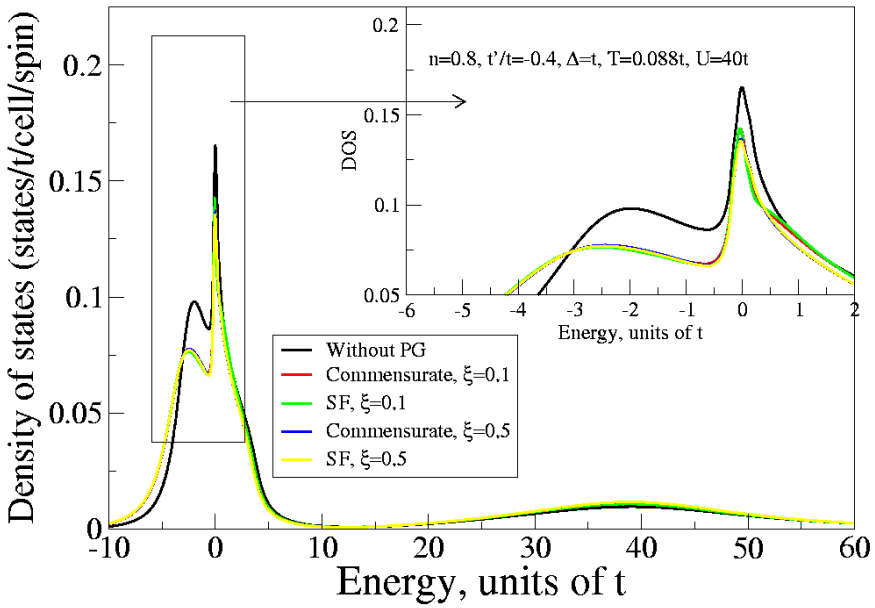

FIG. 3: Comparison of DOSs obtained from DMFT(NRG)+$\Sigma_{\mathbf{k}}$ calculations for $t'/t = -0.4$, $T = 0.088t$, $U = 40t$ and filling $n = 0.8$.

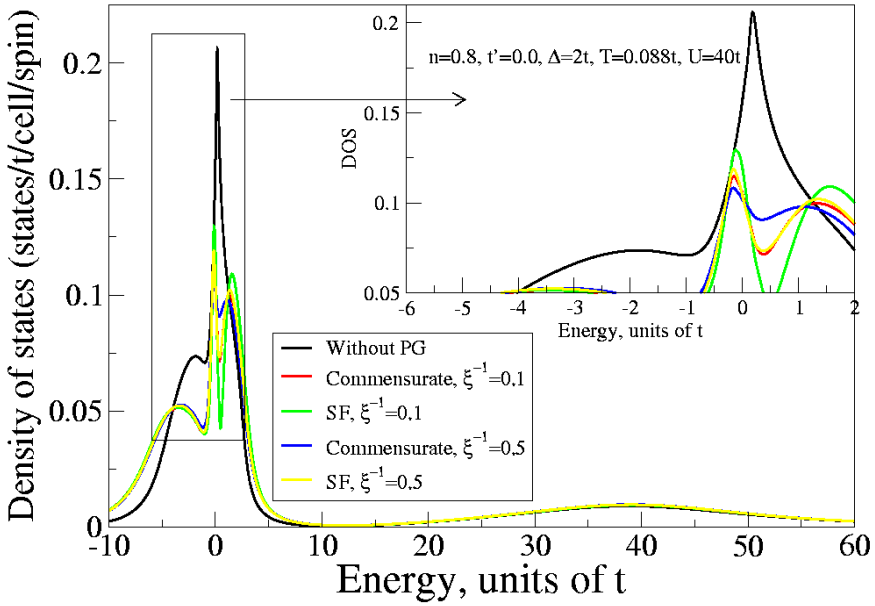

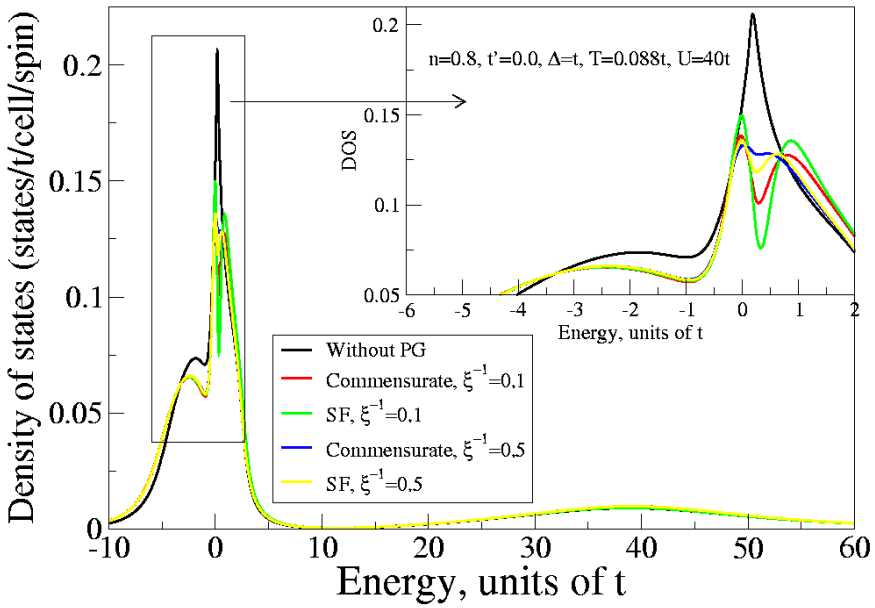

FIG. 4: Comparison of DOSs obtained from DMFT(NRG)+$\Sigma_{\mathbf{k}}$ calculations for $t' = 0$, other parameters as in Fig. 3.

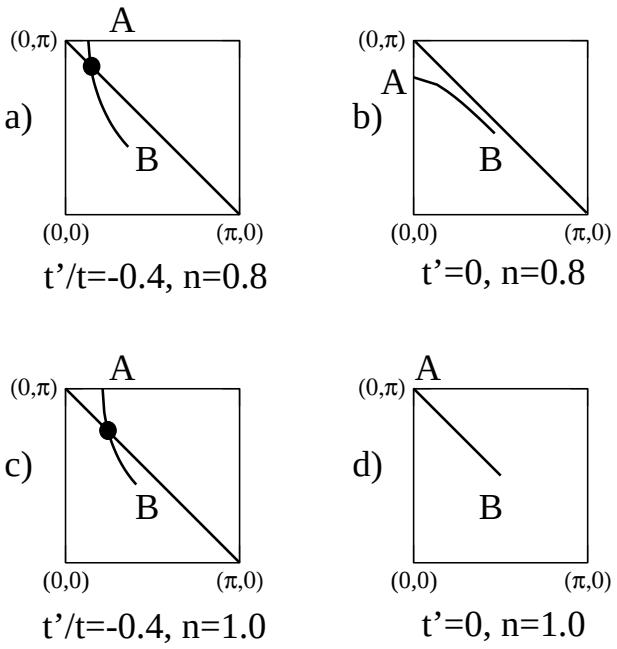

FIG. 5: 1/8-th of the bare Fermi surfaces for the different occupancies n and combinations (t, t') used for the calculation of spectral functions $A(\mathbf{k}, \omega)$. The diagonal line corresponds to the antiferromagnetic Brillouin zone boundary at half–filling for a square lattice with nearest-neighbours hopping only. The full circle marks the so-called "hot–spot".

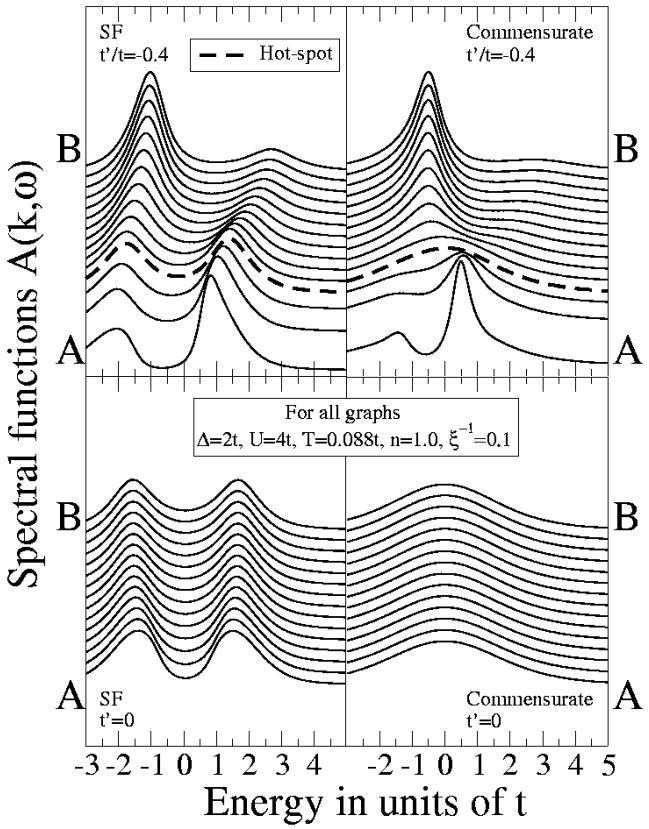

FIG. 6: Spectral functions $A(\mathbf{k},\omega)$ obtained from DMFT(NRG)+$\Sigma_{\mathbf{k}}$ calculations along the directions shown in Fig. 5. Model parameters were chosen as $U = 4t$, $n = 1.0$, $\Delta = 2t$, $\xi^{-1} = 0.1$ and temperature $T = 0.088t$. The "hot–spot" $\mathbf{k}$-point is marked as fat dashed line. The Fermi level corresponds to zero.

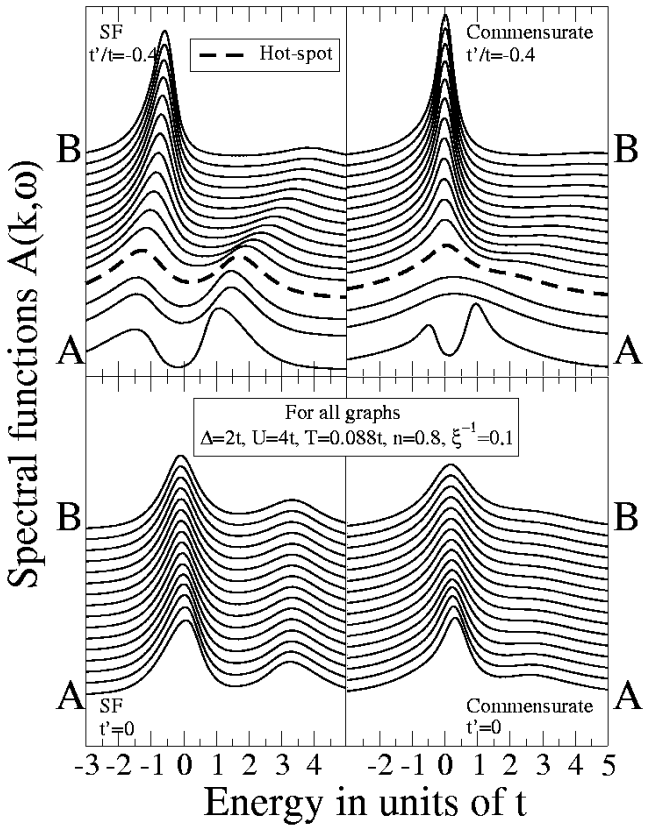

FIG. 7: Spectral functions $A(\mathbf{k},\omega)$ obtained from the DMFT(NRG)+$\Sigma_{\mathbf{k}}$ calculations for $n = 0.8$, other parameters as in Fig. 6.

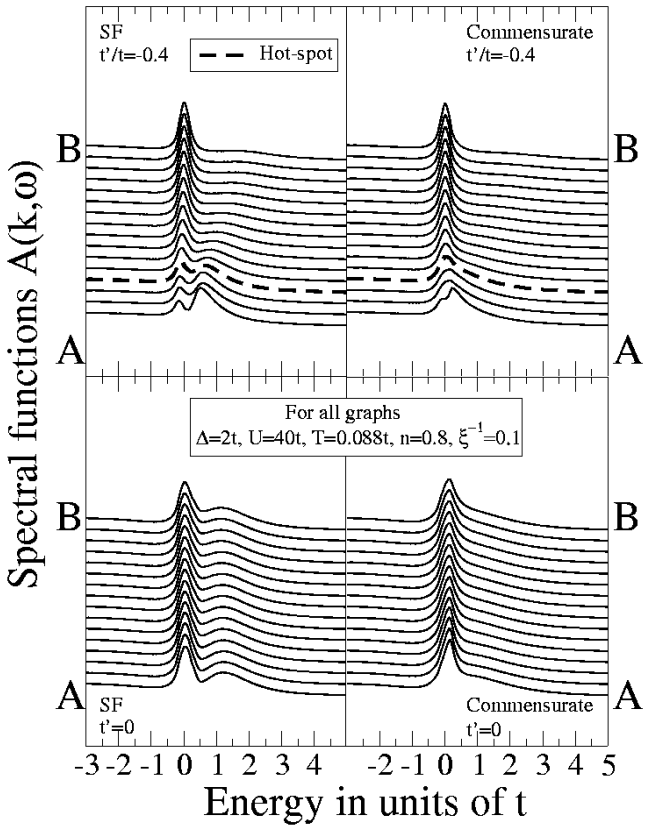

FIG. 8: Spectral functions $A(\mathbf{k},\omega)$ obtained from the DMFT(NRG)+$\Sigma_{\mathbf{k}}$ calculations for $U = 40t$, other parameters as in Fig. 7.

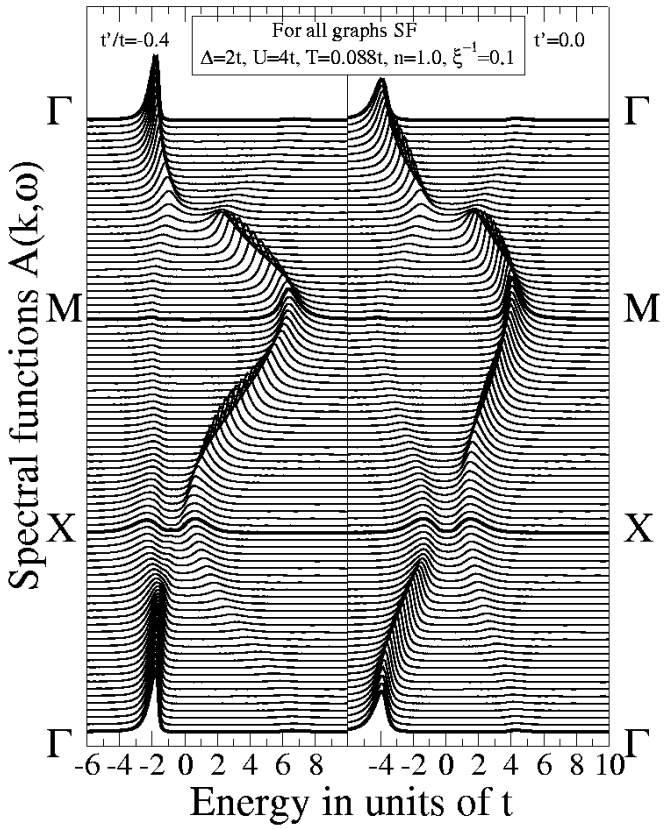

FIG. 9: Spectral functions $A(\mathbf{k},\omega)$ obtained from the DMFT(NRG)+$\Sigma_{\mathbf{k}}$ calculations along high-symmetry directions of first Brilloin zone $\Gamma(0,0)-\mathrm{X}(\pi,0)-\mathrm{M}(\pi,\pi)-\Gamma(0,0)$, SF combinatorics (left row) and commensurate combinatorics (right column). Other parameters are $U = 4t$, $n = 1.0$, $\Delta = 2t$, $\xi^{-1} = 0.1$ and temperature $T = 0.088t$. The Fermi level corresponds to zero.

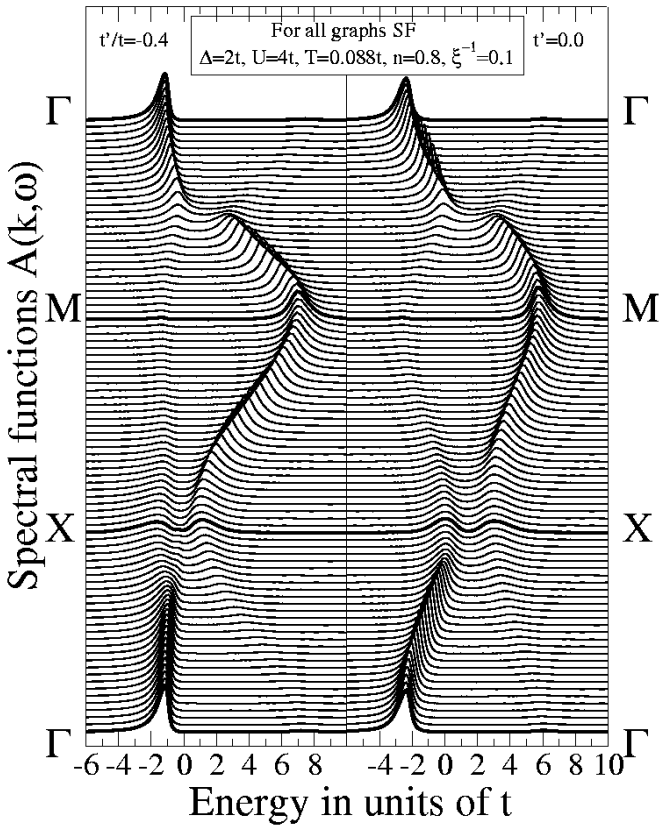

FIG. 10: Spectral functions $A(\mathbf{k},\omega)$ obtained from the DMFT(NRG)+$\Sigma_{\mathbf{k}}$ calculations along high-symmetry lines in the $2D$ Brillouin zone for $n = 0.8$, other parameters as in Fig. 9.

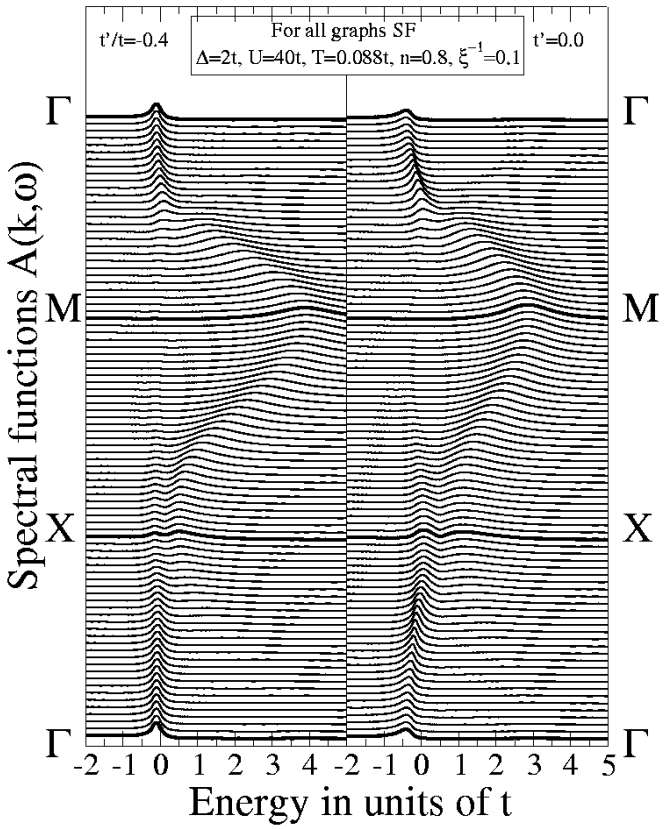

FIG. 11: Spectral functions $A(\mathbf{k},\omega)$ obtained from the DMFT(NRG)+$\Sigma_{\mathbf{k}}$ calculations along high-symmetry lines in the $2D$ Brillouin zone for $U = 40t$, other parameters as in Fig. 10.

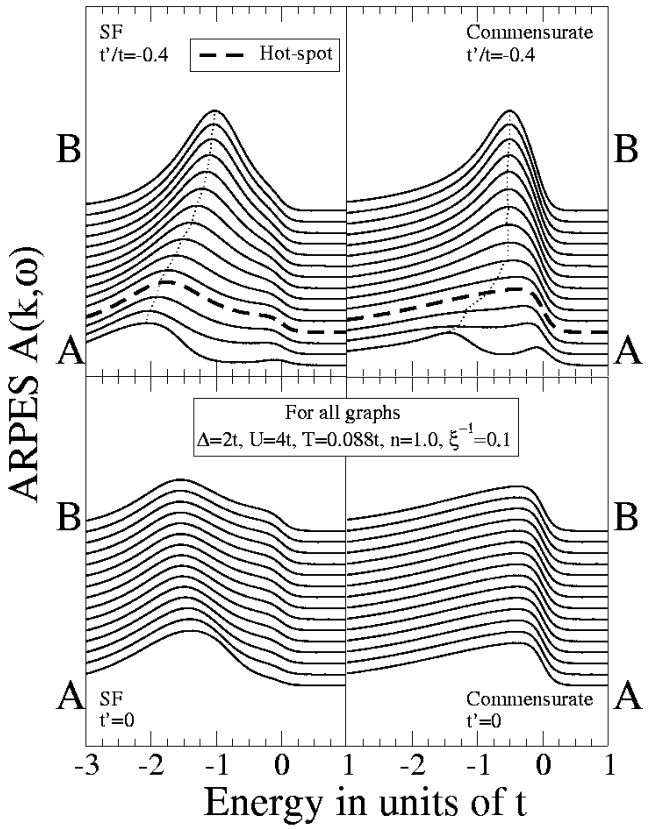

FIG. 12: ARPES obtained from the DMFT(NRG)+$\Sigma_{\mathbf{k}}$ calculations for $U = 4t$ and $n = 1.0$ along the lines in the first BZ as depicted by Fig. 5, all other parameters as in Fig. 6.

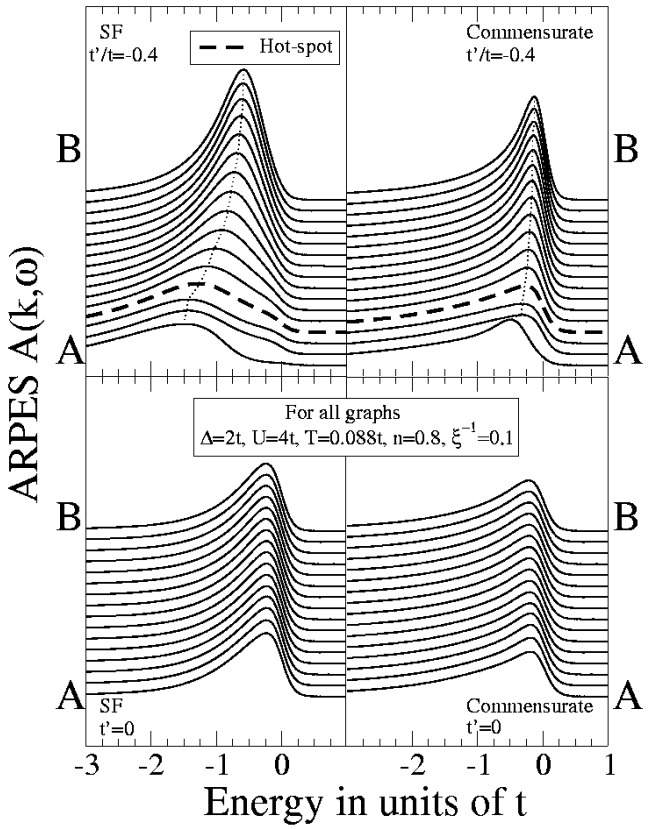

FIG. 13: ARPES obtained from the DMFT(NRG)+$\Sigma_{\mathbf{k}}$ calculations for $U = 4t$ and $n = 0.8$ along the lines in the first BZ as depicted by Fig. 5, all other parameters as in Fig. 7.

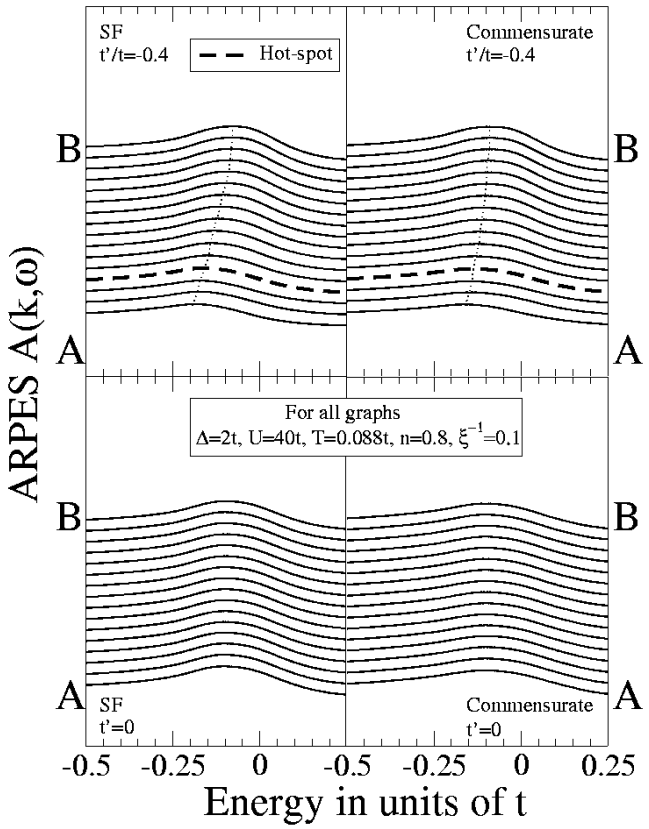

FIG. 14: ARPES obtained from the DMFT(NRG)+$\Sigma_{\mathbf{k}}$ calculations for $U = 40t$ and $n = 0.8$ along the lines in the first BZ as depicted by Fig. 5, all other parameters as in Fig. 8.

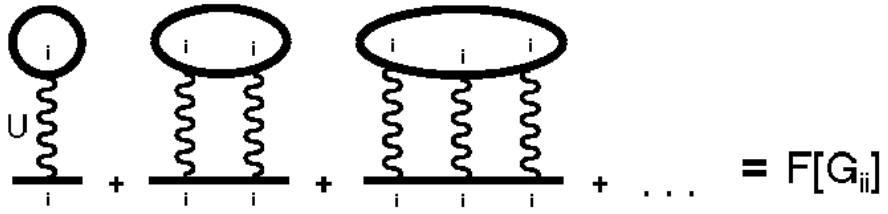

FIG. 15: Local "skeleton" diagrams for the DMFT self–energy Σ. Wavy lines represent the local (Hubbard) Coulomb interaction U, full lines denote the local Green function G_{ii}.

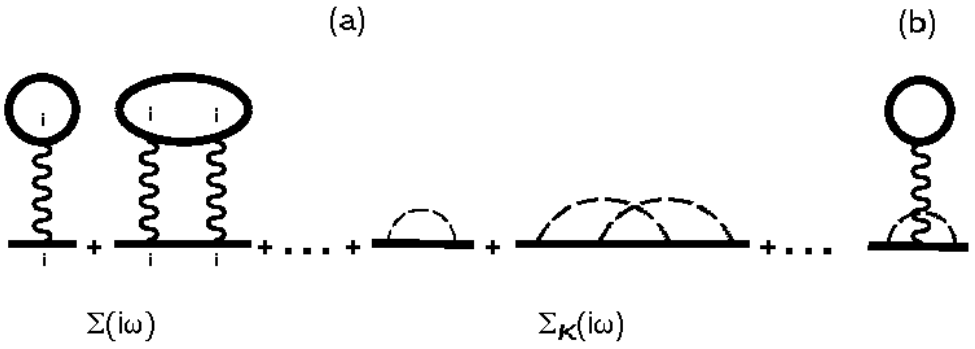

FIG. 16: Typical "skeleton" diagrams for the self–energy in the DMFT+$\Sigma_{\mathbf{k}}$ approach. The first two terms are DMFT self–energy diagrams; the middle two diagrams show contributions to the non-local part of the self–energy from spin fluctuations (see sectionIII) represented as dashed lines; the last diagram (b) is an example of neglected diagramms leading to interference between the local and non-local parts.

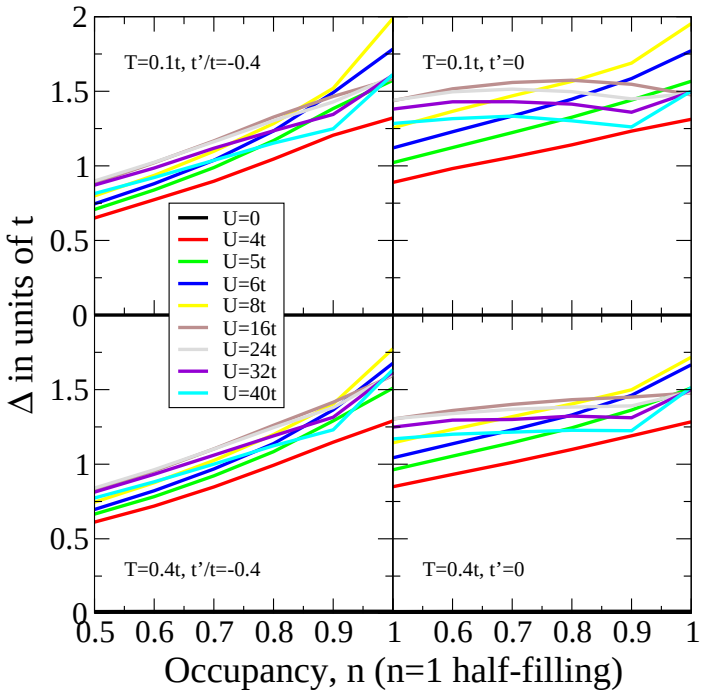

FIG. 17: Filling dependence of the pseudo gap potential Δ calculated with DMFT(QMC) for varying Coulomb interaction (U) and temperature (T) on a two–dimensional square lattice with two sets of (t, t').